Chinese Chemical Letters 33 (2022) 4037–4042

Contents lists available at ScienceDirect

Chinese Chemical Letters

journal homepage: www.elsevier.com/locate/cclet

Novel fast lithium-ion conductor $LiTa_2PO_8$ enhances the performance of poly(ethylene oxide)-based polymer electrolytes in all-solid-state lithium metal batteries

Ying Na[a], Zhe Chen[a], Zhongkai Xu[a], Qi An[a], Xi Zhang[a], Xiaohong Sun[a,*], Shu Cai[a], Chunming Zheng[b,*]

[a] School of Materials Science and Engineering, Key Laboratory of Advanced Ceramics and Machining Technology of Ministry of Education, Tianjin University, Tianjin 300072, China
[b] School of Chemistry and Chemical Engineering, State Key Laboratory of Hollow-fiber Membrane Materials and Membrane Processes, Tiangong University, Tianjin 300387, China

ARTICLE INFO

Article history:
Received 13 October 2021
Revised 29 November 2021
Accepted 10 December 2021
Available online 17 December 2021

Keywords:
Composite solid electrolyte
All-solid-state lithium metal battery
$LiTa_2PO_8$
Poly(ethylene oxide)
Lewis acid

ABSTRACT

At present, replacing the liquid electrolyte in a lithium metal battery with a solid electrolyte is considered to be one of the most powerful strategies to avoid potential safety hazards. Composite solid electrolytes (CPEs) have excellent ionic conductivity and flexibility owing to the combination of functional inorganic materials and polymer solid electrolytes (SPEs). Nevertheless, the ionic conductivity of CPEs is still lower than those of commercial liquid electrolytes, so the development of high-performance CPEs has important practical significance. Herein, a novel fast lithium-ion conductor material $LiTa_2PO_8$ was first filled into poly(ethylene oxide) (PEO)-based SPE, and the optimal ionic conductivity was achieved by filling different concentrations (the ionic conductivity is 4.61×10^{-4} S/cm with a filling content of 15 wt% at 60 °C). The enhancement in ionic conductivity is due to the improvement of PEO chain movement and the promotion of LiTFSI dissociation by $LiTa_2PO_8$. In addition, $LiTa_2PO_8$ also takes the key in enhancing the mechanical strength and thermal stability of CPEs. The assembled $LiFePO_4$ solid-state lithium metal battery displays better rate performance (the specific capacities are as high as 157.3, 152, 142.6, 105 and 53.1 mAh/g under 0.1, 0.2, 0.5, 1 and 2 C at 60 °C, respectively) and higher cycle performance (the capacity retention rate is 86.5% after 200 cycles at 0.5 C and 60 °C). This research demonstrates the feasibility of $LiTa_2PO_8$ as a filler to improve the performance of CPEs, which may provide a fresh platform for developing more advanced solid-state electrolytes.

Recent years have witnessed a spurt of demand for huge energy storage in social development and human life, the growth of power batteries with more reliable safety, higher energy density and longer cycle life has become a new research direction [1]. Lithium metal is considered to be the most ideal anode by reason of its high theoretical capacity (3860 mAh/g) and low standard potential (−3.04 V) [2,3]. Nevertheless, the high reactivity of lithium metal causes side reactions with liquid electrolytes. In particular, uncontrolled accumulation of lithium dendrites can cause a short circuit in the battery [4–6]. In addition, the liquid electrolyte is composed of numerous organic solvents, which can cause serious safety hazards in the application, such as combustion and explosion [7–9]. Accordingly, traditional liquid electrolytes cannot be applied to lithium metal batteries.

The solid electrolyte (SSE) is considered a hopeful candidate material to replace liquid electrolyte by the reason of its great thermal stability, high mechanical strength and good electrochemical stability [10]. Generally, SSEs can be composed of inorganic solid electrolytes (ISEs) and solid polymer electrolytes (SPEs) [11]. ISEs have excellent thermal stability and great ionic conductivity [12]. However, ISEs in the ceramic state do not form good contact with the electrode interface [13,14]. Large interfacial impedance will inhibit the lithium-ion transfer between them, resulting in a battery with low capacity and short cycle life [15]. In contrast, the flexible height of SPEs has a good affinity with electrodes [16]. PEO is the most broadly used SPE at present, but its poor mechanical properties and low ionic conductivity ($\leq 10^{-7}$ S/cm at 25 °C) seriously impede its practical utilization as a single material [17]. In

* Corresponding authors.
E-mail addresses: sunxh@tju.edu.cn (X. Sun), zhengchunming@tiangong.edu.cn (C. Zheng).

https://doi.org/10.1016/j.cclet.2021.12.022
1001-8417/

order to overcome these shortcomings, dispersing inorganic fillers into PEO to form PEO-based CPEs has been manifested to be one of the most valid methods to enhance the capability of all-solid-state lithium metal batteries (ASSLMBs) [18,19]. The introduction of inorganic fillers will reduce the flammability and raise the mechanical properties of the CPE [20,21]. Inorganic fillers are divided into inert fillers (Al_2O_3, TiO_2, SiO_2 and CeO_2, *etc.*) [22–24] and active fillers (perovskite-type, garnet-type and NASICON-type, *etc.*) [25–27]. Notably, active fillers not only enhance the overall Li^+ mobility by enhancing the segment movement of the PEO polymer chain as well as inert fillers, but they also allow rapid Li^+ transport within the ceramic and create fast lithium-ion transport channels at the PEO/ceramic interface, thus achieving extraordinary synergistic effects [28,29].

Although CPEs have the common advantages of ISEs and SPEs, they still have many problems, for instance, poor mechanical performances and low ion conductivity. Hence, there is still a big challenge to develop a CPE with both distinguished electrochemical and safety capabilities. That is, the devise and composite of new materials are of great significance. Recently, Kim *et al.* [30] declared a new solid lithium-ion conductor $LiTa_2PO_8$ (LTPO) with theoretical and practical conductivity of 35.3 mS/cm and 0.25 mS/cm at 25 °C, respectively. It is comparable with $Li_7La_3Zr_2O_{12}$ (garnet-type) and $Li_{3/8}Sr_{7/16}Ta_{3/4}Zr_{1/4}O_3$ (perovskite-type). Furthermore, Fiaz *et al.* [31] used ab initio molecular dynamics simulations to show that the crystal structure of LTPO is very stable during the lithium-ion diffusion process. Its activation energy is only 0.16 eV, which is lower than that of garnet-type $Li_7La_3Zr_2O_{12}$, NASICON-type $LiGe_2(PO_4)_3$ and perovskite-type $Li_{3x}La_{2/3-x}TiO_3$. Meanwhile, Huang *et al.* [32] used LTPO as an inorganic solid electrolyte material to form an ASSLMB (the cathode is $LiFePO_4$). At 55 °C, its specific capacity can still reach 110 mAh/g after 85 cycles under 0.1 mA/cm^2. This work also shows that LTPO exhibits good chemical stability in the air, aqueous solutions and organic solvents, which is better than traditional sulfide and garnet-type solid electrolytes. For example, $Li_{10}GeP_2S_{12}$ has strong hygroscopicity and easily generates toxic hydrogen sulfide gas in contact with moisture [33]. $Li_7La_3Zr_2O_{12}$ forms a Li^+ insulating Li_2CO_3 layer on the surface through H^+/Li^+ exchange, having a large interface impedance [34]. In addition, the commonly studied NASCION-type ($Li_{1+x}Al_xTi_{2-x}(PO_4)_3$) and perovskite-type ($Li_{3x}La_{2/3-x}TiO_3$) electrolytes react with lithium metal to reduce Ti^{4+} to Ti^{3+}, producing electron conduction [35]. The nitride-type (LiPON) is also unstable to metal lithium and the process of assembling the battery is complicated (it needs to be magnetron sputtered to Li anode for use), which limits its large-scale application [36]. All these results have shown that the experimental research of PEO-$LiTa_2PO_8$ CPE is of outstanding significance to broaden the development of ASSLMBs.

Herein, LTPO is first adopted as an active filler in PEO-based solid electrolytes to achieve the best ionic conductivity by filling different concentrations. The results show that 15 wt% LTPO can effectively optimize the ionic conductivity (4.61×10^{-4} S/cm) and lithium-ion mobility (0.448) of the PEO-based solid electrolytes at 60 °C. Importantly, this work has investigated the improvement mechanism of LTPO on PEO-based polymers in detail through various electrochemical, chemical, and mechanical characterizations. For the $LiFePO_4$-ASSLMB assembled by PEO-LiTFSI-15 wt% LTPO CPE, it can achieve better rate performance, higher capacity and longer cycle performance at 60 °C. Further, the uniform lithium metal interface can be observed after cycling, indicating that PEO-LiTFSI-15 wt% LTPO has excellent compatibility with the lithium metal interface. This strategy opens a fresh way for the development of potentially superior performance CPEs.

As shown in Fig. S1a (Supporting information), the prepared LTPO has an irregular particle distribution with a small particle size (~1 μm). The composite membranes with different LTPO content are prepared by the casting method, and they are wrapped by PEO matrix. The XRD patterns of LTPO powders, pure PEO and PEO-LiTFSI-xLTPO (0, 10, 15, 20 and 30 wt%) membranes are presented in Figs. S1b and S2 (Supporting information) and Fig. 1a. The crystal structure of LTPO has almost no impurity phase consistent with previous reports (Fig. S1b) [30,32]. The prepared SSE membranes have a crystalline phase similar to that of PEO, which can be seen by comparison with the XRD pattern of pure PEO (Fig. S2). In addition, it is noteworthy that the characteristic peak intensity of P-Li reduces notably with the increase of LTPO powders doping [37]. Therefore, the introduction of LTPO can lower the crystallinity of PEO obviously, which is conducive to the transfer of Li^+ [38]. It is because of Li^+ coordinates with the ether oxygen atom (-C-O-C) of the PEO segment through complexation in the PEO-based polymer electrolyte [39,40]. These coordinated Li^+ migrate between or within polymer segments and chains as the lithium-oxygen (Li-O) bonds are broken/formed [41,42]. At the same time, the polymer segments rearrange and move to transport Li^+ over long distances. Thus, the increase of the amorphous region in PEO can increase the movement of Li^+ in the electrolyte, that is, the introduction of LTPO is effective [43]. To further observe the SSEs, the surface morphology of the membranes with different LTPO content was characterized by SEM (Figs. 1b-f). These images show that the PEO matrix can be tightly combined with LTPO and the resulting membrane surface is very smooth when LTPO mixing amounts are 10 wt% and 15 wt%. However, when the addition amount reaches 20 wt% or above, the excessive LTPO particles will agglomerate and lead to an uneven surface of the membrane. This is not conducive to the mutual contact between the SSEs and the electrodes and hinders the transmission of Li^+ in the SSE membranes. Especially, element mapping was performed on the P-Li-15LTPO membrane. According to Figs. 1d and g, the elements O, P and Ta are homogeneously distributed in the membrane. Furthermore, the thickness of the P-Li and P-Li-15LTPO membranes are about ~110 μm and ~120 μm, respectively, as shown in Figs. 1h and i.

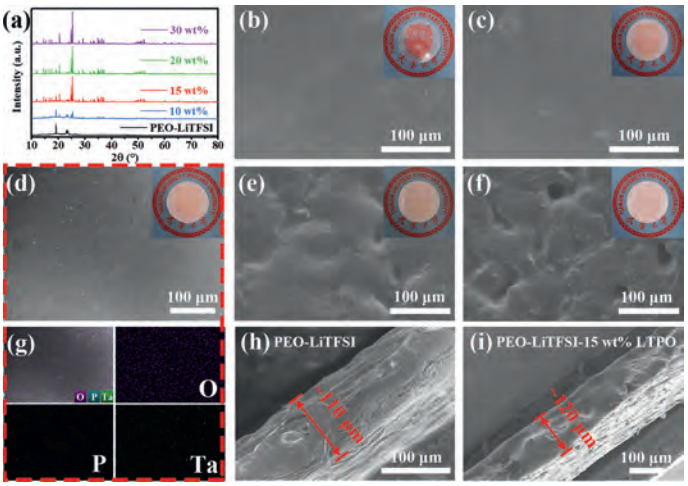

Fig. 1. (a) XRD patterns of PEO-LiTFSI-xLTPO (0, 10, 15, 20 and 30 wt%) membranes. (b-f) Surface SEM images of PEO-LiTFSI-xLTPO (0, 10, 15, 20 and 30 wt%) membranes. (g) Elemental mappings of P-Li-15LTPO membrane. (h, i) The cross-sectional SEM images of P-Li and P-Li-15LTPO membranes.

The thermal stability of SSEs is critical for future applications of high-performance ASSLMBs, especially for safety performance [21,44]. Fig. 2a shows the TGA curves of two SSE membranes (with or without LTPO powders added). The results show that both samples suffered a slight weight loss (2%) below 100 °C, which is attributed to the evaporation of water absorbed from the atmo-

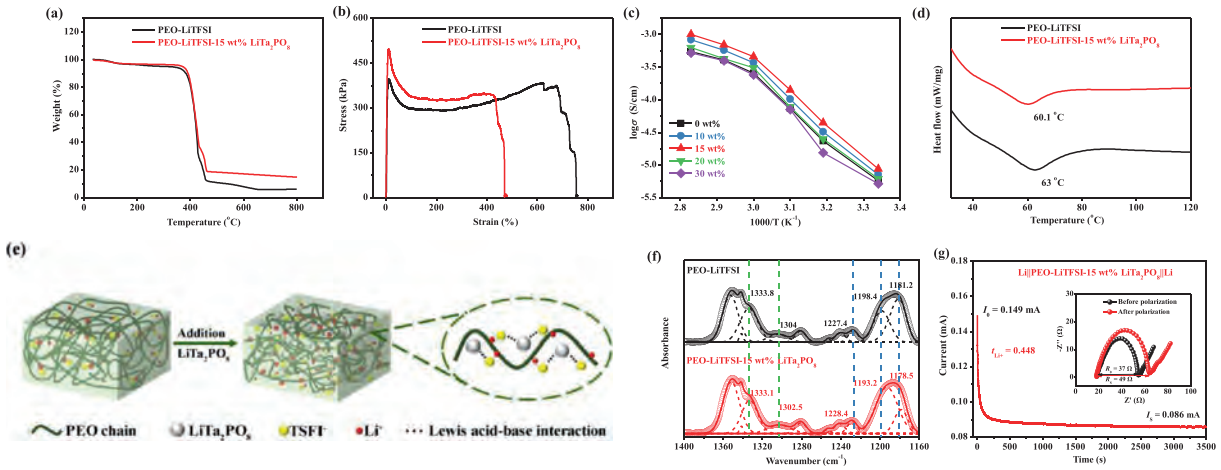

Fig. 2. (a) TGA curves of P-Li and P-Li-15LTPO membranes. (b) Strain-stress curves of P-Li and P-Li-15LTPO membranes. (c) Arrhenius plots of the PEO-LiTFSI-xLTPO (0, 10, 15, 20 and 30 wt%) SSEs at 25–80 °C. (d) DSC curves of P-Li and P-Li-15LTPO SSEs. (e) The mechanism schematic of LTPO in PEO-based electrolyte. (f) FTIR spectra of the P-Li and P-Li-15LTPO SSEs at 1400–1160 cm^{-1}. (g) The chronoamperometry curves of P-Li-15LTPO CPE at a potential step of 10 mV at 60 °C (the inset figure displays EIS of the cell before and after polarization).

sphere. At 350–460 °C, the serious quality loss of both is attributed to the decomposition of PEO and LiTFSI [45]. However, the remaining mass (14.85 wt%) of the P-Li-15LTPO membrane is significantly higher than the P-Li membrane (5.82 wt%) at 800 °C. It is because LTPO still has excellent structural stability and chemical stability at high temperatures. These results demonstrate that LTPO powders can ameliorate the thermal stability of PEO-based electrolytes and prevent the internal short circuit phenomenon of the battery caused by the thermal decomposition of the electrolyte to a certain extent, thereby reducing the occurrence of battery safety accidents. For the sake of more directly observe the stability of the membrane at high temperature, the flammability of conventional liquid electrolytes (1 mol/L $LiPF_6$ in EC/DEC/EMC with equal volume) and SSEs with or without LTPO were compared. As shown in Fig. S3 (Supporting information), the traditional liquid electrolyte burns instantly upon contact with the torch heater and quickly burns into ashes. P-Li and P-Li-15LTPO membranes are ignited after 10 s but do not burn continuously (the flame goes out instantly as soon as it leaves the torch heater). After the burning test, the P-Li membrane has many holes and cannot maintain its original shape to become a viscous liquid. Inversely, the P-Li-15LTPO membrane only has a hole in the place where the fire is most prosperous, and it can almost maintain its integrity. Thus, the addition of LTPO powders can maintain the shape of PEO-based electrolytes at high temperatures and improve the safety of ASSLMBs.

Moreover, the security performance of ASSLMBs is also related to the mechanical performance of SSEs [46]. Electrolyte membranes with high mechanical properties can restrain the continuous growth of lithium dendrites and prevent ASSLMBs from short-circuiting. Therefore, the P-Li and P-Li-15LTPO membranes were subjected to tensile tests, and the strain-stress curves obtained are shown in Fig. 2b. The results display that the tensile strength of the P-Li-15LTPO membrane is 496.54 KPa, which is higher than the 393.56 KPa of the P-Li membrane. Furthermore, P-Li-15LTPO membrane also has a high plastic strain, nearly 479%. In simple terms, LTPO ceramics can effectively inhibit dendrites as a physical barrier, thus improving the operating stability of batteries. The above results fully demonstrate that the P-Li-15LTPO membrane can be used as a safe and reliable CPE in an ASSLMB.

In addition to the above two properties, the electrochemical performances of SSEs are also very important for batteries in practical applications. Firstly, the AC impedance characterization of SSEs with different contents of LTPO was carried out at 25 °C (Fig. S4 in Supporting information). Among all the samples, the minimum impedance of the sample containing 15 wt% LTPO powders is about 815 Ω less than 1065 Ω for P-Li. Fig. 2c is the Arrhenius plots of SSEs with different LTPO contents at 25–80 °C. It is obvious that the ionic conductivity (σ) enhances with increasing temperature. when the doping amount reaches 15 wt%, the σ of SSE is about twice that of P-Li SSE (4.61×10^{-4} S/cm *vs.* 2.38×10^{-4} S/cm, at 60 °C). Combined with previous studies on the modification mechanism of CPEs, the theory of LTPO powders in PEO-based electrolytes is devised and explained in three aspects [47,48]. First, LTPO inorganic powders can remarkably reduce the crystallinity of PEO and strength the segment movement of the polymer, thereby improving the overall ionic conductivity. This explanation can be confirmed by combining the XRD patterns earlier and the following DSC. Fig. 2d gives the DSC curves of two SSE membranes with and without LTPO. It can be seen that the melting transition (T_m) of SSE decreased from 63 °C to 60.1 °C after adding LTPO powders. This further proves that the additive LTPO does decrease the crystallinity of PEO and promote ion migration [49]. Second, there is a strong interaction between the Lewis acid center of LTPO and $TFSI^-$, which leads to the separation of Li^+ from LiTFSI to release more Li^+ (Fig. 2e) [20,50-52]. To confirm this hypothesis, FTIR tests were performed on samples with and without LTPO. Fig. S5 (Supporting information) and Fig. 2f demonstrate the complete (4000–400 cm^{-1}) and detailed (1400–1150 cm^{-1}) FTIR spectra of LTPO, P-Li and P-Li-15LTPO, respectively. Among them, the peaks near 1351, 1342, 1280 and 1241 cm^{-1} are attributed to pure PEO, and the other peaks belong to the symmetrical and asymmetrical stretching of -SO_2- and -CF_3 groups in LiTFSI. By comparison, when 15 wt% LTPO ceramic powders were added, the peak of -SO_2- asymmetric stretching at 1333.8 and 1304 cm^{-1} moved to 1333.1 and 1302.5 cm^{-1}, respectively. Meanwhile, the peaks of -CF_3 symmetric stretching at 1227.4 cm^{-1} moved to 1228.4 cm^{-1}, and the peaks of -CF_3 asymmetric stretching at 1198.4 and 1181.2 cm^{-1} migrated to 1193.2 and 1178.5 cm^{-1}, separately. The changes of -SO_2- and -CF_3 group peaks indicate that there is a strong interaction between LTPO fillers and LiTFSI. Hence, the introduction of LTPO can promote the divorce of the LiTFSI and release more Li^+ to increase the ionic conductivity. Finally, the large number of Lewis acid sites on the LTPO can facilitate Li^+ migration at the phase interface between the PEO and LTPO [20]. However, excessive addition of LTPO will result in a decrease in the σ of SSEs (>15 wt%). This is because the entire area where ions migrate

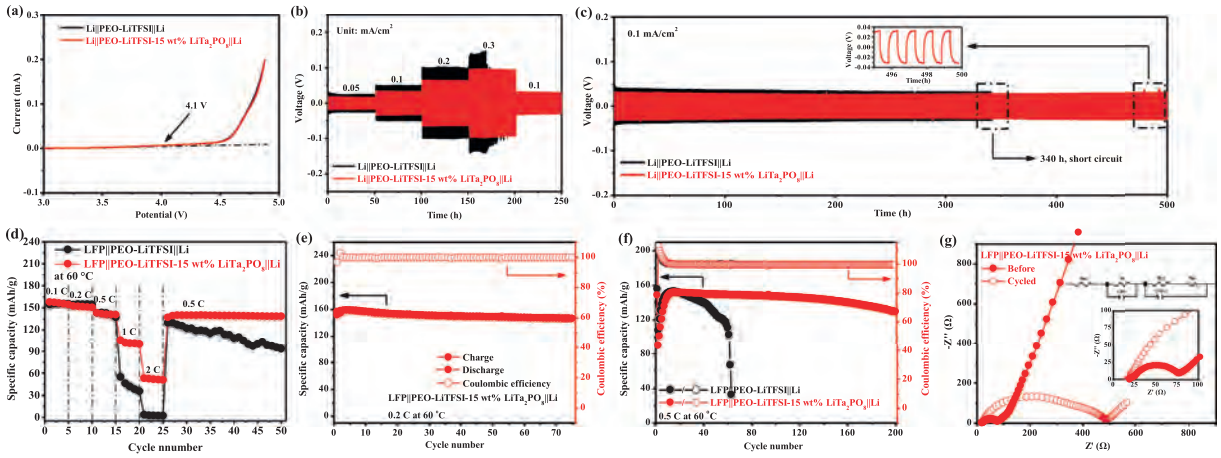

Fig. 3. (a) LSV plots of P-Li and P-Li-15LTPO SSEs at 1.0 mV/s. (b) Galvanostatic cycling curves of Li||P-Li||Li and Li||P-Li-15LTPO||Li cells at different current densities. (c) Galvanostatic cycling curves of Li metal plating/stripping under 0.1 mA/cm^2 (the inset shows a magnified plot from 495 h to 500 h). (d) Rate performance of LFP||P-Li||Li and LFP||P-Li-15LTPO||Li cells. (e) Cycle performance of LFP||P-Li-15LTPO||Li cell at 0.2 C. (f) Long cycling performance of LFP||P-Li||Li and LFP||P-Li-15LTPO||Li cells. (g) EIS of LFP||P-Li-15LTPO||Li cell before and after 200 cycles. All tests are performed at 60 °C.

in the CPE contains the polymer, the active fillers, and the interface phase between the polymer and the active fillers [53]. In this system, first of all, excessive LTPO leads to a reduction in the miscibility of PEO and LTPO, hindering the transfer of ions in the polymer [8,10]. It can also be obtained from the above analysis of the SEM images. Secondly, an appropriate amount of LTPO forms a connected percolation network to support the diffusion of ions through the LTPO phase, while excessive LTPO causes irregular agglomeration effects and hinders the diffusion of ions [54]. Finally, the clustering phenomenon caused by excessive LTPO can also cause a sharp reduction in the volume ratio of the interface between the polymer and the active fillers, which leads to a significant decrease in ionic conductivity [55]. Fig. 2g and Fig. S6 (Supporting information) respectively show the DC polarization curve and the AC impedance spectrum of the Li||SSE||Li cells composed of two SSEs (P-Li and P-Li-15LTPO SSEs). The results display that the t_{Li^+} of P-Li-15LTPO CPE is 0.448, much higher than that of P-Li SSE (0.141). The increase in t_{Li^+} is going to be attributed to the interaction between LTPO and -SO_2- and -CF_3 groups in LiTFSI, which can also be proved by the FTIR analysis above.

Another important factor of ASSLMBs is the electrochemical stability under working voltage [56]. For the sake of determining the working voltage range of the sample, the electrochemical window of the SS||SSE||Li cells was studied using LSV at 60 °C. As exhibited in Fig. 3a, the initial decomposition potential of P-Li-15LTPO CPE is similar to that of P-Li SSE, about 4.1 V. It is due to the stable electrochemical window of LTPO ceramic powders being 2.01 ~4.01 V [31]. To further explore the interface stability of SSE membranes/lithium metal, the lithium plating/stripping behavior of the two SSE membranes was measured at different current densities by assembling Li||SSE||Li cells (0.05, 0.1, 0.2 and 0.3 mA/cm^2 at 60 °C). Fig. 3b describes that Li||P-Li-15LTPO||Li cell presents a lower polarization voltage at all current densities and generates a more favorable electrolyte/lithium anode interface. Inversely, Li||P-Li||Li cell produces a greater polarization and short-circuit at 0.3 mA/cm^2. Otherwise, for the long-cycle lithium plating/peeling behavior test at 0.1 mA/cm^2, Li||P-Li-15LTPO||Li cell also shows better stability (Fig. 3c). Li||P-Li||Li cell has a short circuit after 340 h, while Li||P-Li-15LTPO||Li cell has a stable cycle for more than 500 h and its lithium plating/stripping overpotential remains at ~32 mV. The lithium symmetry test shows that the prepared P-Li-15LTPO CPE has good stability with the lithium metal anode. Appropriately, the SSE can be paired with a lithium metal anode to build an advanced ASSLMB.

The ASSLMBs with lithium metal anodes, LFP cathodes and P-Li or P-Li-15LTPO electrolytes were constructed. Fig. 3d exhibits the rate performance of LFP||P-Li||Li and LFP||P-Li-15LTPO||Li cells at 60 °C. The initial discharge specific capacity of LFP||P-Li-15LTPO||Li cell is 157.3, 152, 142.6, 105 and 53.1 mAh/g at 0.1, 0.2, 0.5, 1 and 2 C, respectively. Almost all higher than LFP||P-Li||Li cell (153.9, 152.1, 142.6, 55 and 13.4 mAh/g), especially at high rates. It proves that the mixture of LTPO powders can greatly optimize the rate capacity. As the current density is readjusted to 0.5 C, the battery containing LTPO can still provide a high discharge capacity of 136.3 mAh/g and can be kept stably, while the capacity of the battery without LTPO is only 128.9 mAh/g and decays gradually. Additionally, according to the corresponding charge and discharge curves (Fig. S7 in Supporting information), the overpotential of the two batteries will increase with the increase of current density. As a stark comparison, ASSLMB using P-Li-15LTPO electrolyte has low voltage polarization and a flat working platform. It indicates that LTPO can improve interface compatibility of the electrolyte/electrode, which is beneficial to the stability of the battery.

The long-term cycle properties of LFP||P-Li||Li and LFP||P-Li-15LTPO||Li cells are illustrated in Figs. 3e and f. At low current density (0.2 C), LFP||P-Li-15LTPO||Li cell delivers stable cycling properties (Fig. 3e). Its initial discharge capacity is 150.9 mAh/g, and the capacity retention rate can attain 97% after 70 cycles. At high current densities (0.5 C), both batteries provide lower capacity in the first cycle, implying an active process (Fig. 3f). Meanwhile, the coulombic efficiency of the two batteries in the early stage is higher than 100%. This is because the cathode not only inserts the originally extracted lithium but also inserts the lithium provided by the lithium metal during the early discharge process, which leads to this phenomenon [20,57,58]. In particular, LFP||P-Li-15LTPO||Li cell exhibits ultrahigh specific discharge capacity of 128.4 mAh/g after 200 cycles, and the capacity retention rate is close to 86.5%. For LFP||P-Li||Li cell, its discharge specific capacity decayed rapidly from 151.4 mAh/g to 109.9 mAh/g within 60 cycles, and then a short-circuit occurred. Due to the violent polarization between P-Li SSE and lithium metal along with the continuous generation of lithium dendrites during the cycle, a large number of deposited lithium dendrites break through the electrolyte and cause a short circuit eventually. By contrast, the LFP||P-Li-15LTPO||Li cell still displays a constant voltage polarization after

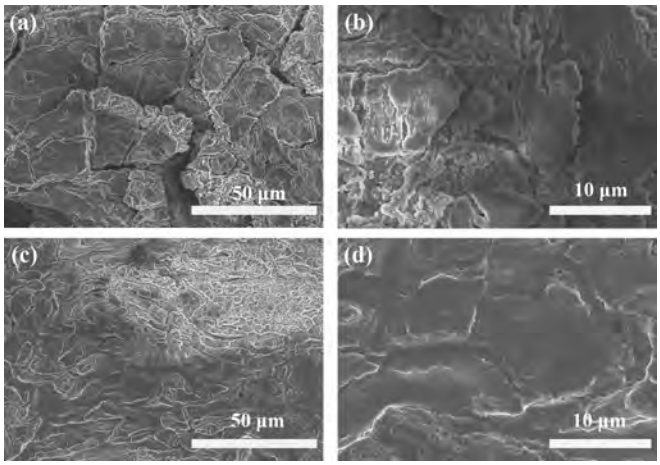

Fig. 4. Surface SEM images of Li anodes in the (a, b) LFP||P-Li||Li and (c, d) LFP||P-Li-15LTPO||Li cells after 200 cycles at 0.5 C.

200 cycles (Fig. S8 in Supporting information). Obviously, ASSLMB composed of P-Li-15LTPO has better cycle performance. It can be attributed to two aspects [59,60]. On the one hand, the LTPO ceramic powders enhance the mechanical strength of the SSE, so that it has enough stress to hinder the penetration of lithium dendrites. This guarantees battery stability during long-term cycling. On the other hand, LTPO ceramic powders can decrease the crystallinity of the polymer and release more Li^+ *via* Lewis acidsites effectively, thereby raising the ionic conductivity and t_{Li^+} of the SSE. This can improve battery cycle performance greatly.

The cycle performance is also approximately related to the interface stability of the electrolyte/electrode [61]. Perform EIS on LFP||P-Li||Li and LFP||P-Li-15LTPO||Li cells before and after the cycle, as demonstrated in Fig. 3g and Fig. S9 (Supporting information). Compared with P-Li SSE, the ASSLMB composed of P-Li-15LTPO CPE has a smaller resistance (62.05 Ω *vs.* 66.81 Ω). Furthermore, the resistance of LFP||P-Li-15LTPO||Li cell changes slightly after cycling (476.16 Ω *vs*. 2332 Ω). In other words, the addition of 15 wt% LTPO improves the interface compatibility of solid electrolyte/electrode, enhancing the cycle performance of the battery greatly [62]. Fig. 4 displays the SEM images of lithium metal anodes in LFP||P-Li||Li and LFP||P-Li-15LTPO||Li cells after long loop. The results show that the lithium anode surface from the battery without LTPO is uneven and possesses large quantities of lithium dendrites. On the contrary, the lithium anode from the battery containing LTPO has a relatively flat surface and a small number of lithium dendrites. These results are in accordance with the electrochemical test consequences, indicating that the SSE containing LTPO can effectively prevent the growth of lithium dendrites. The inhibition ability of P-Li-15LTPO CPE on lithium dendrites growth can be ascribed to its excellent ionic conductivity and mechanical strength [63,64]. Among them, the higher ionic conductivity can facilitate the rapid diffusion of Li^+ in the electrolyte, so that the Li deposition is uniform. Meanwhile, sufficient mechanical strength inhibits the lithium dendrites' growth and avoids the occurrence of short circuits. These excellent electrochemical properties prove that LTPO ceramic powders as an active additive effectively strengths the electrochemical properties of PEO-based electrolytes, and the ASSLMBs composed of them also have high development potential.

In all, we analyze the effect of LTPO powers on the physical and electrochemical performances of PEO-based electrolytes and determine the optimal addition amount. The results show that 15 wt% LTPO as filler could effectively lower the crystallinity of PEO and enhance the ionic conductivity of the SSE (4.61×10^{-4} S/cm). Meanwhile, based on Lewis acid-base theory, the strong adsorption of LTPO powders on $TFSI^-$ promotes the release and convey of Li^+, thereby enhancing the migration number of Li^+ in the SSE ($t_{Li^+} = 0.448$). Moreover, by reason of the high strength and flame retardancy of the LTPO powders additive, the mechanical properties and thermal stability of the SSE are improved. The $LiFePO_4$-ASSLMB assembled by PEO-LiTFSI-15 wt% LTPO CPE also displays remarkable rate performance and cycle performance. It has high specific capacities of 157.3, 152, 142.6, 105 and 53.1 mAh/g under 0.1, 0.2, 0.5, 1 and 2 C at 60 °C. After 200 cycles at 0.5 C and 60 °C, it still delivers an excellent discharge specific capacity of 128.4 mAh/g. Hence, LTPO as an active filler can effectively optimize the properties of SSEs, which opens a new way for the development of potential ASSLMBs with superior performance.

Declaration of competing interest

The authors declare that they have no known competing financial interests or personal relationships that could have appeared to influence the work reported in this paper.

Acknowledgments

This work was supported by the National Natural Science Foundation of China (NSFC, Nos. 52073212, 51772205, 51772208), and the General Program of Municipal Natural Science Foundation of Tianjin (Nos. 17JCYBJC17000, 17JCYBJC22700).

Supplementary materials

Supplementary material associated with this article can be found, in the online version, at doi:10.1016/j.cclet.2021.12.022.

Reference

[1] L. Chen, W. Li, L. Fan, et al., Adv. Funct. Mater. 29 (2019) 1901047.
[2] X. Cheng, R. Zhang, C. Zhao, et al., Chem. Rev. 117 (2017) 10403–10473.
[3] R. Zhang, N. Li, X. Cheng, et al., Adv. Sci. 4 (2017) 1600445.
[4] G. Cui, Matter 2 (2020) 805–815.
[5] Q. Zhou, S. Dong, Z. Lv, et al., Adv. Energy Mater. 10 (2020) 1903441.
[6] X. Ren, S. Chen, H. Lee, et al., Chem 4 (2018) 1877–1892.
[7] H. Yang, J. Bright, B. Chen, et al., J. Mater. Chem. A 8 (2020) 7261–7272.
[8] J. Zheng, M. Tang, Y. Hu, Angew. Chem. Int. Ed. 128 (2016) 12726–12730.
[9] Q. Wang, Z. Cui, Q. Zhou, et al., Energy Stor. Mater. 25 (2020) 756–763.
[10] W. Zhang, J. Nie, F. Li, et al., Nano Energy 45 (2018) 413–419.
[11] J. Janek, W.G. Zeier, Nat. Energy 1 (2016) 16141.
[12] X. Han, Y. Gong, K.K. Fu, et al., Nat. Mater. 16 (2017) 572–579.
[13] W. Luo, Y. Gong, Y. Zhu, et al., Adv. Mater. 29 (2017) 1606042.
[14] Q. Wang, H. Zhang, Z. Cui, et al., Energy Stor. Mater. 23 (2019) 466–490.
[15] Z. Zhang, Y. Shao, B. Lotsch, et al., Energy Environ. Sci. 11 (2018) 1945–1976.
[16] Y. Li, W. Zhang, Q. Dou, et al., J. Mater. Chem. A 7 (2019) 3391–3398.
[17] Z. Xue, D. He, X. Xie, J. Mater. Chem. A 3 (2015) 19218–19253.
[18] Z. Wan, D. Lei, W. Yang, et al., Adv. Funct. Mater. 29 (2019).
[19] J. Hu, P. He, B. Zhang, et al., Energy Stor. Mater. 26 (2020) 283–289.
[20] O. Sheng, C. Jin, J. Luo, et al., Nano Lett. 18 (2018) 3104–3112.
[21] J. Wen, R. Zhang, Q. Zhao, et al., ACS Appl. Mater. Interfaces 12 (2020) 54637–54643.
[22] T. Liu, J. Zheng, H. Hu, et al., J. Energy Chem. 55 (2021) 272–278.
[23] Y. Liu, Y. Wu, J. Zheng, et al., Nano Energy 82 (2021) 105723.
[24] S. Abinaya, H.P. Kavitha, M. Prakash, et al., Sustain. Chem. Pharm. 19 (2021).
[25] W. Wang, E. Yi, A.J. Fici, et al., J. Phys. Chem. C 121 (2017) 2563–2573.
[26] Y. Jung, S. Lee, J. Choi, et al., J. Electrochem. Soc. 162 (2015) A704–A710.
[27] M. Keller, G.B. Appetecchi, G. Kim, et al., J. Power Sources 353 (2017) 287–297.
[28] W. Liu, D. Lin, J. Sun, et al., ACS Nano 10 (2016) 11407–11413.
[29] N. Wu, P. Chien, Y. Qian, et al., Angew. Chem. Int. Ed. 59 (2020) 4131–4137.
[30] J. Kim, J. Kim, M. Avdeev, et al., J. Mater. Chem. A 6 (2018) 22478–22482.
[31] F. Hussain, P. Li, Z. Li, J. Phys. Chem. A 123 (2019) 19282–19287.
[32] B. Huang, B. Xu, J. Zhang, et al., J. Mater. Sci. 56 (2021) 2425–2434.
[33] N. Kamaya, K. Homma, Y. Yamakawa, et al., Nat. Mater. 10 (2011) 682–686.
[34] J. Wolfenstine, J.L. Allen, J. Read, et al., J. Mater. Sci. 48 (2013) 5846–5851.
[35] A. Belous, G. Kolbasov, L. Kovalenko, et al., J. Solid State Electrochem. 22 (2018) 2315–2320.
[36] S. Nowak, F. Berkemeier, G. Schmitz, J. Power Sources 275 (2015) 144–150.
[37] W. Liu, N. Liu, J. Sun, et al., Nano Lett. 15 (2015) 2740–2745.
[38] X. Wang, Y. Zhang, X. Zhang, et al., ACS Appl. Mater. Interfaces 10 (2018) 24791–24798.

[39] F. Croce, G. Appetecchi, L. Persi, et al., Nature 394 (1998) 456–458.
[40] A. Stephan, Eur. Polym. J. 42 (2006) 21–42.
[41] K. Xu, Chem. Rev. 104 (2004) 4303–4417.
[42] W. Meyer, Adv. Mater. 10 (1998) 439.
[43] M. Dirican, C. Yan, P. Zhu, et al., Mater. Sci. Eng. R Rep. 136 (2019) 27–46.
[44] Q. Zhang, X. Zhang, H. Yuan, et al., Small Sci. 1 (2021) 2100058.
[45] H. Chen, D. Adekoya, L. Hencz, et al., Adv. Energy Mater. 10 (2020) 2000049.
[46] W. Zhou, S. Wang, Y. Li, et al., J. Am. Chem. Soc. 138 (2016) 9385–9388.
[47] Y. Zhang, R. Chen, S. Wang, et al., Energy Stor. Mater. 25 (2020) 145–153.
[48] Z. Shen, Y. Cheng, S. Sun, et al., Carbon Energy 3 (2021) 482–508.
[49] L. Chen, Y. Li, S. Li, et al., Nano Energy 46 (2018) 176–184.
[50] X. Zheng, K. Liu, T. Yang, et al., J. Alloys Compd. 877 (2021) 160307.
[51] Z. Wang, X. Huang, L. Chen, Electrochem. Solid-State Lett. 6 (2003) E40–E44.
[52] B. Zhao, L. Ma, K. Wu, et al., Chin. Chem. Lett. 32 (2021) 125–131.
[53] W. Wang, E. Yi, A.J. Fici, et al., J. Phys. Chem. C 121 (2017) 2563–2573.
[54] Z. Shen, Y. Cheng, S. Sun, et al., Carbon Energy 3 (2021) 482–508.
[55] A.J. Bhattacharyya, J. Maier, Adv. Mater. 16 (2004) 811.
[56] X. Yao, D. Liu, C. Wang, et al., Nano Lett. 16 (2016) 7148–7154.
[57] L. Gao, H. Liang, J. Li, et al., J. Power Sources 515 (2021) 230622.
[58] X. Hao, Q. Zhao, S. Su, et al., Adv. Energy Mater. 9 (2019) 1901604.
[59] J. Shim, H.J. Kim, B.G. Kim, et al., Energy Environ. Sci. 10 (2017) 1911–1916.
[60] K. Oh, D. Lee, M. Choo, et al., ACS Appl. Mater. Interfaces 6 (2014) 7751–7758.
[61] J. Ding, R. Xu, C. Yan, et al., J. Energ. Chem. 59 (2021) 306–319.
[62] Z. Wan, D. Lei, W. Yang, et al., Adv. Funct. Mater. 29 (2019) 1805301.
[63] D. Zhou, R. Liu, Y. He, et al., Adv. Energy Mater. 6 (2016) 1502214.
[64] Y. Liu, D. Lin, P.Y. Yuen, et al., Adv. Mater. 29 (2017) 1605531.